Crystallographic and magnetic structure of $SrCoO_{2.5}$ brownmillerite: Neutron study coupled with band-structure calculations

A. Muñoz,[1,*] C. de la Calle,[2] J. A. Alonso,[2] P. M. Botta,[3] V. Pardo,[3] D. Baldomir,[3] and J. Rivas[3]
[1]*Departamento de Física Aplicada, EPS, Universidad Carlos III, Avenida Universidad 30, E-28911, Leganés-Madrid, Spain*
[2]*Instituto de Ciencia de los Materiales de Madrid, CSIC, E-28049, Cantoblanco-Madrid, Spain*
[3]*Departamento de Física Aplicada, Facultad de Física, Universidad de Santiago de Compostela, E-15782 Campus Sur s/n, Santiago de Compostela, Spain*

(Received 20 December 2007; revised manuscript received 2 June 2008; published 5 August 2008)

A study of the crystallographic and magnetic structure of $SrCoO_{2.5}$ with a brownmillerite-type structure has been carried out from neutron powder-diffraction (NPD) measurements at temperatures ranging from 10 to 623 K, across the Néel temperature (T_N=537 K) of this antiferromagnetic oxide. The study has been complemented with differential scanning calorimeter (DSC), *dc* susceptibility and magnetization measurements. Although the refinement of the crystal structure from NPD data is possible in the orthorhombic *Pnma* and *Ima*2 space groups, the support of *ab-initio* band-structure calculations has allowed us to select, without ambiguity, the *Ima*2 space group as the ground state for $SrCoO_{2.5}$ brownmillerite. In *Ima*2 the crystallographic structure of $SrCoO_{2.5}$ is described as layers of corner-sharing $Co1O_6$ octahedra alternating along the *a* axis with layers of vertex-sharing $Co2O_4$ tetrahedra, conforming chains running along the [0 0 1] direction. The magnetic structure below T_N=537 K is *G*-type with the magnetic moments directed along the *c* axis. This magnetic arrangement is stable from T_N down to 10 K. At T=10 K, the magnetic moment values for Co1 and Co2 atoms are $3.12(13)\mu_B$ and $2.88(14)\mu_B$, respectively, compatible with a $Co^{2+}\underline{L}$ state, where $\underline{L}$ stands for a ligand hole. The magnetic susceptibility curves show, below 200 K, a divergence of zero-field cooling and field cooling curves, displaying broad maxima which are interpreted as due to the presence of ferromagnetic clusters embedded into an antiferromagnetic matrix. These inhomogeneities are inherent to the synthesis process, by quenching microcrystalline samples of $SrCoO_{3-x}$ composition from high temperature, where cubic, ferromagnetic perovskites have been identified by diffraction methods.

DOI: 10.1103/PhysRevB.78.054404 PACS number(s): 75.25.+z

I. INTRODUCTION

Among the nonstoichiometric $ABO_{3-\delta}$ perovskite oxides, $SrCoO_{3-\delta}$ presents a rich phase diagram, exhibiting different crystal structures as a function of the oxygen deficiency and also depending even on the preparative conditions.[1–3] Some of the materials of this system have been recently receiving much attention since for certain compositions $SrCoO_{3-x}$ displays a high oxygen mobility at room temperature, what makes it a very suitable compound for different technical applications such as gas sensing probes or oxygen membranes, with application in solid oxide fuel cells.[4,5]

The nearly stoichiometric $SrCoO_3$ phase can be prepared under high oxygen pressure;[2] Bezdicka *et al.*[6] and Le Toquin *et al.*[7] also proposed the synthesis of the fully stoichiometric $SrCoO_3$ using electrochemical oxidation of $SrCoO_{2.5}$ (or $Sr_2Co_2O_5$) brownmillerite phase. Although $SrCoO_{2.5}$ is metastable at room temperature, the brownmillerite-type structure can be stabilized by quenching $SrCoO_{3-\delta}$ from 1000 °C, in air, into liquid nitrogen.[1,8] The quenching process procures the ordering of the oxygen vacancies. On heating $SrCoO_{2.5}$ from room temperature, different intermediate rhombohedral phases appear and finally, at around 900 °C, the structure becomes cubic.[9,10]

The $SrCoO_{2.5}$ brownmillerite is a superstructure of perovskite due to the long-range ordering of the 0.5 oxygen vacancies per formula unit. Its crystal structure can be obtained from the perovskite structure ABO_3 by removing one third of the oxygen atoms in every second (*h*00) layer of octahedra in an ordered way along the [100] cubic direction. Therefore, the structure of $SrCoO_{2.5}$ can be described as a stacking of layers of CoO_4 tetrahedra alternating with layers of CoO_6 octahedra along the *a* axis, with the Sr atoms located in the voids between the polyhedra. The lattice parameters of the orthorhombic unit cell of $SrCoO_{2.5}$ are related to the lattice parameters of the cubic perovskite unit cell by $a_o \approx 4a_p$, $b_o \approx \sqrt{2}a_p$, and $c_o \approx \sqrt{2}a_p$. The assignment of space group to $SrCoO_{2.5}$ has been controversial; in fact, $A_2B_2O_5$ compounds with brownmillerite structure have been described to crystallize in different orthorhombic space groups, *Pnma* (no. 62), *Ima*2 (no. 46) and *Imma* (no. 74), depending on the metal composition and temperature; in some cases, as in $Ca_2Fe_2O_5$, there has been some ambiguity in the assignment of the space group due to the weakness of the $h+k+1 \neq 2n$ Bragg reflections.[11] Let us point out that the different orthorhombic space groups only imply slight differences in the arrangement of the BO_4 tetrahedral chains. In a recent study,[7] the *Pnma* space group has been proposed for $SrCoO_{2.5}$ at room temperature; according to the same study, the intermediate $SrCoO_{2.75}$ and $SrCoO_{2.82}$ phases crystallize in the cubic *Pm*-3*m* and tetragonal *I*4/*mmm* space groups, respectively.

Magnetic measurements indicate that $SrCoO_{2.5}$ (Ref. 12) undergoes a long-range antiferromagnetic (AFM) order below T_N=570 K. In this paper *ab-initio* band-structure calculations allowed us to identify the *Ima*2 space group as the ground state for the crystal and magnetic structure of $SrCoO_{2.5}$ brownmillerite; thus we have investigated by neutron powder-diffraction (NPD) the thermal evolution of the

crystal and magnetic structures of $SrCoO_{2.5}$ in the 10–623 K temperature range, in complement with magnetization measurements. We also give an interpretation of the divergence of the zero-field cooling (ZFC) and field cooling (FC) curves at ~200 K, which is not due to any change in the magnetic structure of brownmillerite but is originated by the presence of ferromagnetic (FM) clusters in an AFM matrix.

II. EXPERIMENTAL

A. Sample preparation

$SrCoO_{2.5}$ was obtained as a polycrystalline sample by a citrate technique. Stoichiometric amounts of analytical grade $Sr(NO_3)_2$ and $Co(NO_3)_2 \cdot 6H_2O$ were dissolved in a citric acid concentrated aqueous solution. The so-formed organic resin was dried at 140 °C and slowly decomposed at temperatures up to 600 °C for 12 h. The sample was then heated at 900 °C for 12 h in air. The brownmillerite-type structure was obtained by quenching the sample from this temperature in liquid N_2.

B. X-ray and neutron diffraction, magnetic measurements and thermal analysis

The reaction products were characterized by x-ray diffraction (XRD) for phase identification and to assess phase purity. The characterization was performed using a Bruker-AXS D8 diffractometer (40 kV, 30 mA) in Bragg-Brentano reflection geometry with CuK_α radiation ($\lambda = 1.5418$ Å).

The NPD experiments were carried out at the Institut Laue-Langevin, Grenoble (France). Different patterns were collected at 295 K (RT), 373 K, 473 K and 623 K at the D1A diffractometer with a $\lambda = 1.91$ Å wavelength; above RT the sample was contained in a quartz tube open to the air atmosphere, placed in a vanadium furnace. Additionally, a low-temperature NPD pattern was obtained at $T = 10$ K with $\lambda = 1.594$ Å at the D2B diffractometer. The different NPD diagrams were refined by using the Rietveld method[13] with the FULLPROF program.[14] The profile of the Bragg reflections was simulated with a pseudo-Voigt function; the background was fitted either with a fifth-degree polynomial function (NPD patterns collected at RT and $T = 10$ K) or by linear interpolation from a high number of points of the background.

The magnetic measurements of $SrCoO_{2.5}$ were performed in a sample property measuring system (SPMS) from Quantum Design. The *dc* magnetization was measured both in ZFC and FC conditions. Three susceptibility curves were obtained in the temperature interval $5 < T < 320$ K under a magnetic field of 0.1, 0.5, and 1 kOe. Above RT, an additional susceptibility curve was obtained in the $300 < T < 700$ range under 1 kOe. Different magnetization curves were measured at $T = 25$ K and $T = 220$ K for magnetic fields ranging from-10 kOe to 10 kOe.

Thermal analysis was performed with a differential scanning calorimeter (DSC) from Perkin Elmer. A small pellet of $SrCoO_{2.5}$ (28 mg) was heated from RT up to 720 K using a heating rate of 20 $K.min^{-1}$ and a N_2 flowing atmosphere.

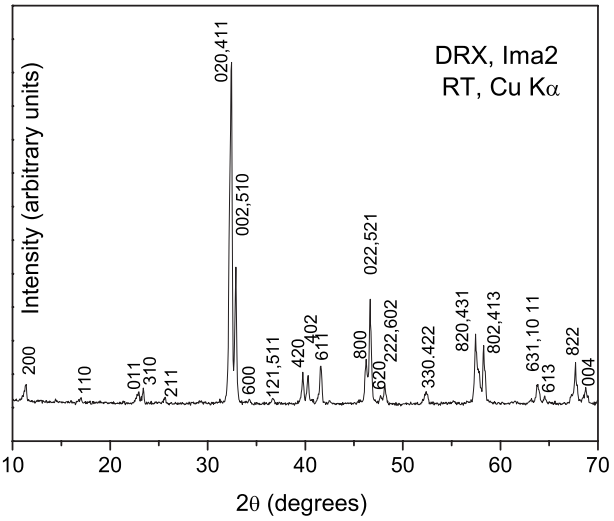

FIG. 1. XRD pattern for $SrCoO_{2.5}$ brownmillerite, indexed in an orthorhombic unit cell with $a = 5.4579(3)$, $b = 15.6388(10)$, $c = 5.5643(3)$Å, space group *Ima*2.

C. Computational details

Full potential, all electron, electronic structure calculations based on the density functional theory (DFT) utilizing the APW+lo method[15] were performed using the WIEN2K software.[16] We have included the strong correlation effects to deal with the Co *d* electrons by means of the LDA+U scheme.[17] The nonorbitally dependent part of the exchange-correlation functional was modeled using the Perdew-Burke-Ernzerhof generalized gradient approximation (GGA) scheme.[18] Spin-orbit effects have been introduced in a second variational way using the scalar relativistic approximation.[19] We have converged all our calculations with respect to the *k*-mesh and to $R_{mt} * K_{max}$, up to 82 *k*-points in the irreducible wedge of the Brillouin zone: a $3 \times 9 \times 9$ mesh and up to $R_{mt} * K_{max} = 7$. Local orbitals were added for a bigger flexibility in dealing with the semicore states. Muffin-tin radii chosen were the following: 2.28 a.u. for Sr, 1.79 a.u. for Co, and 1.59 a.u. for O.

III. RESULTS

A. X-ray diffraction, thermal analysis and magnetic measurements

$SrCoO_{2.5}$ was obtained as a pure, well-crystallized brownmillerite phase; Figure 1 shows the XRD pattern, indexed in an orthorhombic unit cell with $a = 15.7450(5)$, $b = 5.5739(2)$, $c = 5.4697(2)$ Å. There are no traces of the competitive hexagonal phase with the same composition, which can be obtained by slow cooling of the same precursor oxides from 900 °C in air.

The thermal evolution of the ZFC and FC magnetization curves of $SrCoO_{2.5}$ measured between 0.1 and 1 kOe are compared in Fig. 2, in the temperature range 5 to 320 K. In complement, a DSC thermogram measured above RT is displayed in Fig. 3. An endothermic peak centered at 537 K is observed. The inset shows the *dc* magnetic susceptibility, revealing a clear inflection about the same temperature. This

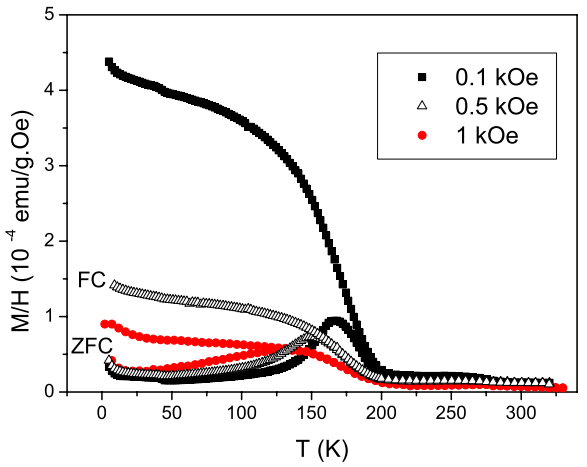

FIG. 2. (Color online) Thermal evolution of the FC and ZFC *dc* susceptibility obtained under different magnetic fields.

is in good agreement with the reported Néel temperature for $SrCoO_{2.5}$, T_N=570 K.[12] On decreasing the temperature below 200 K (Fig. 2) the susceptibility of both ZFC curves increase, displaying a broad maximum, the cusp of which is shifted to lower temperatures for higher applied fields. The FC curves diverge from the corresponding ZFC curves below 170 K (H=0.1 kOe) and 140 K (H=1 kOe). Besides, at low temperature, the FC curves show a thermal evolution characteristic of a FM ordering. This behavior can be clearly observed in the isothermal magnetization curves shown in Fig. 4. At 25 K hysteresis is observed, although the remnant magnetization is very small, $0.002\mu_B$ per formula. At 220 K an almost linear response characteristic of an AFM material is observed. This behavior already suggests the presence of weak FM interactions, which are overimposed to the long-range antiferromagnetic ordering established below 537 K.

B. Crystallographic structure from neutron powder-diffraction data

As it has been indicated in Sec. I, there was a serious ambiguity related to the assignment of the orthorhombic

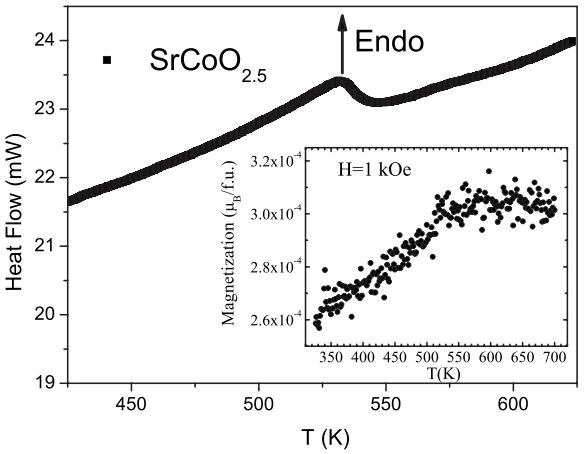

FIG. 3. DSC curve for $SrCoO_{2.5}$ recorded above room temperature. The inset shows the variation of the magnetic susceptibility in the same temperature range.

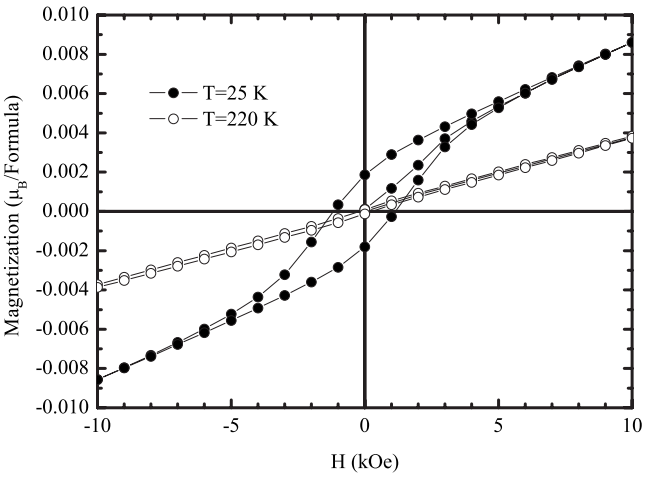

FIG. 4. Isothermal magnetization curves at T=25 and 220 K.

space group for $SrCoO_{2.5}$ with brownmillerite structure; therefore, both the orthorhombic space group *Ima*2 and *Pnma* have been initially taken into consideration. The main difference between both groups is that the inversion symmetry element is present in *Pnma* whereas *Ima*2 is a noncentrosymmetric space group. This fact determines the orientation of the CoO_4 tetrahedral chains along the longest lattice parameter, *a* for *Ima*2 and *b* for *Pnma*; as it can be seen in Fig. 5(a), for the space group *Ima*2 the octahedral chains placed at x=0.25 and x=0.75 display the same orientation, shifted by (1/2,1/2,1/2). However, for the space group *Pnma*, the octahedral chain placed at y=0.25 exhibits a different orientation from that placed at y=0.75 due to the fact that both chains are related by the inversion symmetry element.

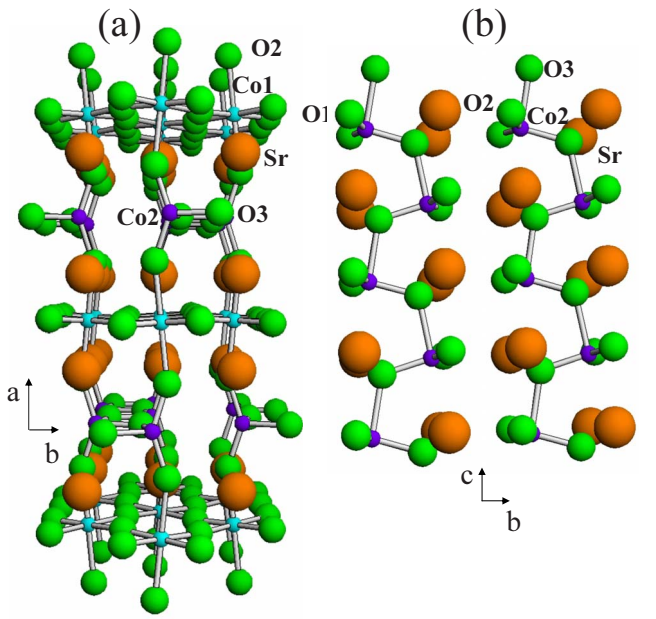

FIG. 5. (Color online) Views of the brownmillerite-type structure of $SrCoO_{2.5}$ defined in the orthorhombic *Ima*2 space group: a) Layers of $Co1O_6$ octahedra and $Co2O_4$ tetrahedra alternate along the [100] direction. b) Chains of $Co2O_4$ tetrahedra are running along [001] direction.

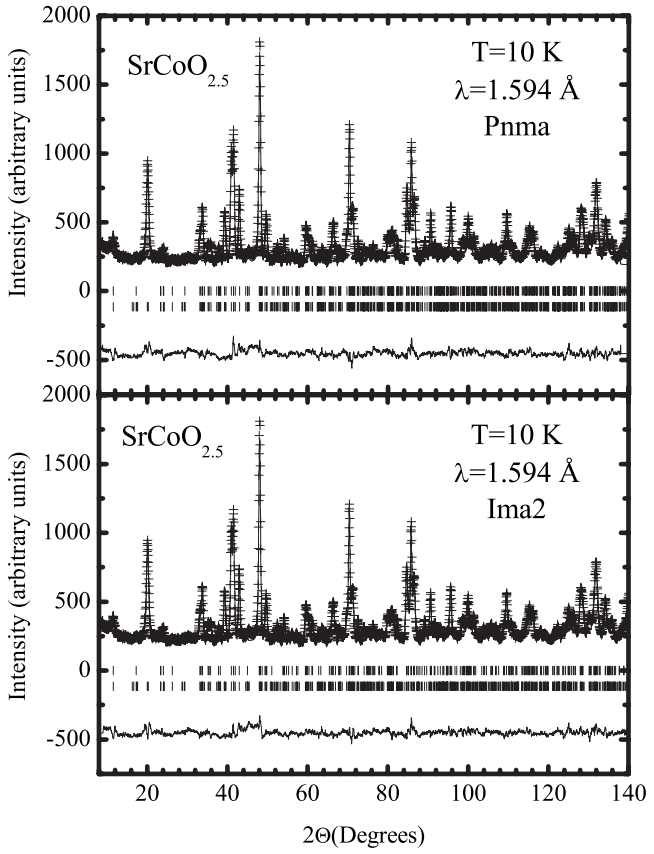

FIG. 6. Comparison of the observed (crosses), calculated (solid line) and difference (at the bottom) NPD patterns at $T=10$ K; the first and second rows of tick marks correspond, respectively, to the nuclear and magnetic reflections. (a) *Pnma* space group. (b) *Ima*2 space group.

Also, Fig. 5(b) illustrates the chains of $Co2O_4$ tetrahedra, linked through O3 oxygens, running along the c axis in the *Ima*2 space group.

In a first trial, we performed the refinement of the crystal structure from NPD data at $T=10$ K, at both space groups *Pnma* and *Ima*2. The Rietveld plots are displayed in Fig. 6, showing in both cases a satisfactory agreement between the experimental and calculated diagrams. The introduction of the magnetic structure was required to complete the fitting of the NPD patterns, as described below. Table I contains the main structural parameters in both space groups at 10 K. The subtle difference between the refinements in both space groups concerns the *hkl* Bragg reflections that verify the relationship $h+k+l=2n+1$, which are forbidden for the space group *Ima*2; however, these reflections are too weak to be clearly observed and it is not possible to decide between both space groups from the quality of the crystal structure refinements.

At $T=10$ K $SrCoO_{2.5}$ is magnetically ordered; for the space group *Pnma* the magnetic reflections are explained by using the propagation vector $\mathbf{k}=0$; in case that the space group *Ima*2 is considered to define the crystallographic structure, the magnetic peaks can be indexed by using the propagation vector $\mathbf{k}=(1,1,1)$. In both cases the magnetic contribution to the calculated NPD patterns has been taken into account. Again, the fit of the magnetic structures in both space groups is equally possible, leading to similar Bragg R factors, and describing a globally identical magnetic coupling of the Co spins. To solve this dilemma we have been strongly supported by the *ab-initio* calculations described below, which clearly and unambiguously show a by far higher stability of the *Ima*2 crystal structure. Therefore the orthorhombic *Ima*2 space group has been selected for the refinement of the crystal and magnetic structures from the NPD patterns acquired at 10, 295, 373, 473, and 623 K. The

TABLE I. Atomic positions, lattice parameters and discrepancy factors for the refinement of the crystallographic structure of $SrCoO_{2.5}$. In the orthorhombic space group *Pnma* (10 K) Sr, O1 and O2 are at 8d (x,y,z), Co1 at 4a (0,0,0) and CO2 and O3 at 4c (x,1/4,z). In the space group *Ima*2 (10 K and 295 K), Sr, O1 and O2 are at 8c (x,y,z), Co1 at 4a (0,0,0) and Co2 and O3 at 4b (1/4,y,z). At $T=295$ K the magnetic R_{Bragg} factor is 9.3 %.

Lattice parameters		10 K *Pnma*	10 K *Ima*2	295 K *Ima*2
a(Å)		5.4579(3)	15.6376(7)	15.7450(5)
b(Å)		15.6388(10)	5.5644(3)	5.5739(2)
c(Å)		5.5643(3)	5.4580(2)	5.4697(2)
Vol(Å^3)		474.94(8)	474.92(4)	480.03(3)
R_P(%)		5.3	4.9	5.5
R_{wp}(%)		6.7	6.3	6.9
R_{Bragg}(%)		8.9	8.6	5.5
χ^2		1.5	1.3	1.7
Atom position				
Sr	x	0.4981(13)	0.1104(1)	0.11125(11)
	y	0.1102(2)	0.0111(6)	0.0085(5)
	z	0.0107(6)	0.517(3)	0.503(5)
	B(Å)	0.02(2)	0.02(2)	0.46(5)
Co1	x	0.000	0.000	0.000
	y	0.000	0.000	0.000
	z	0.000	0.000	0.000
	B(Å)	0.02(2)	0.02(2)	0.41(14)
Co2	x	0.020(3)	0.25	0.25
	y	0.25	0.942(2)	0.938(2)
	z	0.943(2)	0.045(4)	0.033(6)
	B(Å)	0.02(2)	0.02(2)	0.41(14)
O1	x	0.2575(12)	0.9951(3)	0.9946(3)
	y	0.9940(3)	0.2439(12)	0.2534(12)
	z	0.2526(15)	0.253(3)	0.250(4)
	B(Å)	0.02(2)	0.02(2)	0.66(6)
O2	x	-0.0013(15)	0.1407(2)	0.1421(2)
	y	0.1409(2)	0.0408(5)	0.0391(6)
	z	0.0422(5)	0.018(3)	0.009(5)
	B(Å)	0.02(2)	0.02(2)	0.79(7)
O3	x	0.6239(10)	0.25	0.25
	y	0.25	0.8705(10)	0.8684(10)
	z	0.8694(11)	0.641(4)	0.631(5)
	B(Å)	0.02(2)	0.0(2)	1.05(12)

TABLE II. Bonding distances (in Å) and angles (in degrees) corresponding to the CoO_6 octahedron and CoO_4 tetrahedron for $SrCoO_{2.5}$, at 10 K and 295 K (space group *Ima*2).

Bonding distances	10 K	295 K
Co1-O1(x2)	1.938(14)	1.970(10)
Co1-O1(x2)	1.963(13)	1.939(10)
Co1-O2(x2)	2.214(3)	2.249(3)
⟨Co1-O⟩	2.038(10)	2.053(7)
Co2-O2(x2)	1.801(5)	1.794(5)
Co2-O3	2.25(3)	2.23(4)
Co2-O3	1.815(14)	1.788(10)
⟨Co2-O⟩	1.917(14)	1.901(15)
Bonding angles		
Co1-O1-Co1	175.1(6)	175.0(8)
Co1-O2-Co2	156.2(2)	155.9(2)
Co2-O3-Co2	116.8(9)	117.4(9)

atomic parameters and the most important bonding distances and the bonding angles concerning the $Co1O_6$ octahedra and $Co2O_4$ tetrahedra at 10 K and 295 K are listed in Tables I and II. The evolution of the crystal structure above 295 K is described elsewhere.[10]

C. Magnetic structure resolution details

Upon decreasing the temperature below T_N=537 K new reflections of magnetic origin appear on the NPD patterns, as shown in Fig. 7. As mentioned before, for the space group *Ima*2 the new reflections of magnetic origin are indexed with the propagation vector $\mathbf{k}=(1,1,1)$. The possible magnetic structures compatible with the crystal symmetry have been determined by following the method described by Bertaut.[20] The possible magnetic modes for $\mathbf{k}=(1,1,1)$ and for the 4*a*

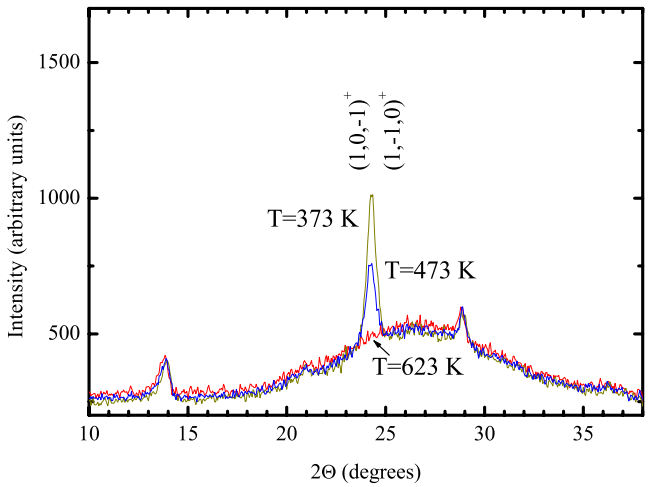

FIG. 7. (Color online) Thermal evolution of the NPD patterns collected at T=373, 473, and 623 K with λ=1.91 Å. Only the angular range around the $(1,0,-1)^+$ and $(1,-1,0)^+$ magnetic reflections is represented.

TABLE III. Magnetic structures obtained for the space group *Ima*2 and $\mathbf{k}=(1,1,1)$. The atoms of the 4*a* site are denoted as: Co1 (0,0,0), Co2 (1/2,0,0). For the 4*b* site the notation is: Co3 (1/4,y,z), Co4 $(3/4,-y,z)$.

	4*a*		4*b*	
Representation	Co1	Co2	Co3	Co4
Γ_1	(0,0,1)	(0,0,−1)	(1,0,0)	(−1,0,0)
Γ_2	(0,0,1)	(0,0,1)	(0,1,1)	(0,−1,1)
Γ_3	(1,1,0)	(−1,1,0)	(0,1,1)	(0,1,−1)
Γ_4	(1,1,0)	(1,−1,0)	(1,0,0)	(1,0,0)

and 4*b* sites occupied by the Co atoms are given in Table III. After checking the different solutions in the ordered region, the best agreement with the experimental results is obtained for the magnetic modes corresponding to the Γ^2 irreducible representation; although for this irreducible representation the basis vectors for the atoms of the 4*b* site imply a possible magnetic component along the *y* direction; after the refinement from the different NPD diagrams this m_y magnetic component turns to be negligible and, therefore, the magnetic moments of the Co atoms in both sites are oriented along the *z* direction. The coupling of the magnetic moment is $m_{1z}=m_{2z}$ for the Co atoms of the 4*a* site, and $m_{3z}=m_{4z}$ for the Co atoms of the 4*b* site. The Co atoms which are obtained by a (1/2,1/2,1/2) translation from the Co1 and Co2, and Co3 and Co4 are antiferromagnetically coupled with respect to the initial Co atom. A plot of the magnetic arrangement of the Co spins is shown in Fig. 8; it can be described as a *G*-type magnetic structure with AFM layers of CoO_6 octahedra alternating along the *a* direction with AFM layers of CoO_4 tetrahedra; the coupling of the octahedral and tetrahedral layers is also AFM. The thermal evolution of the ordered magnetic moments at the octahedral and tetrahedral positions is displayed in Fig. 9. At T=10 K, the magnetic moment values for Co1 and Co2 atoms are $3.12(13)\mu_B$ and $2.88(14)\mu_B$, respectively, for the 4*a* and 4*b* sites.

D. Electronic structure calculations

We have performed electronic structure calculations in the two possible structures at low temperature (T=10 K), with

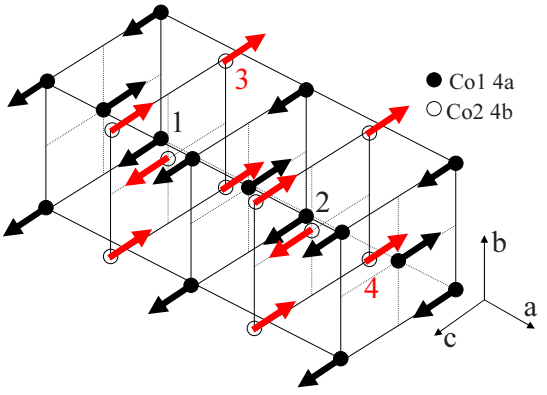

FIG. 8. (Color online) A view of the magnetic structure of $SrCoO_{2.5}$ below T_N=537 K. For sake of clarity, only the Co atoms are represented.

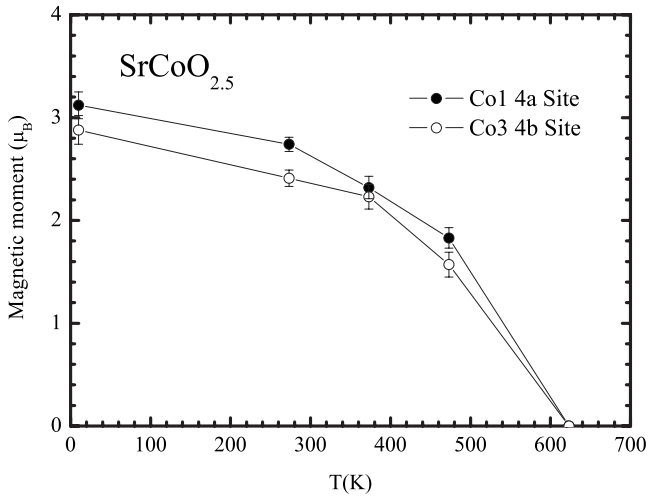

FIG. 9. Thermal evolutions of the magnetic moments of the Co atoms placed at the 4*a* and 4*b* sites.

space groups *Pnma* and *Ima*2, based upon the atomic parameters listed in Tables I and II. We have always considered the experimentally found AFM *G*-type structure, with the magnetization pointing along the *c* axis (in the *Ima*2 setting). The total energy in both possible structures for various values of the effective on-site Coulomb repulsion U was computed. The absolute value of the total energies does not have an intrinsic physical sense, because it depends on many parameters of the calculation (number of local orbitals added, linearization energies, *k*-points mesh, energy cutoff for the core states, number of plane waves utilized, etc.), which all have been previously converged to yield reliable results. The same set of parameters was used for each space group with the aim to make the calculation independent from these variables. For this reason we show the difference between the total energies instead of the absolute energy values. For $U=0$, the *Ima*2-based structure is more stable than the one based on the *Pnma* space group by 34 meV/Co. When strong correlations are taken into account, the *Ima*2 structure gets stabilized even further (by 400 meV/Co when $U=3$ eV and by 550 meV/Co for $U=5$ eV). These results leave no doubt about the much higher stability of the *Ima*2-based structure with respect to the other possible space group.

We have also carried out the relaxation of the structure of $SrCoO_{2.5}$ within both space groups. For that sake, we have started from our experimentally obtained lattice parameters and atomic positions and relaxed both the volume and the internal atomic positions. The main conclusion remains unchanged, i.e., the *Ima*2 space group is more stable than the *Pnma*. Our results show that the structure within the *Pnma* space group relaxes to a volume 3% higher than experiment, whereas within the *Ima*2 space group, it relaxes to the experimental volume (within less than 1% accuracy). The total energy difference between both relaxed structures is approximately 64 meV/Co within GGA and, when strong correlation effects are considered by means of the LDA+U scheme, the energy difference reduces to about 36 meV/Co for $U=5$ eV, which is qualitatively equivalent to the results obtained with the experimental structures.

IV. DISCUSSION

Ab-initio electronic structure calculations demonstrate that the crystallographic structure of $SrCoO_{2.5}$ is orthorhombic, *Ima*2 space group. In principle, the orthorhombic *Pnma* space group also seems to be compatible with the NPD data, but the total energy of this structure is considerably higher. The crystallographic structure of $SrCoO_{2.5}$ can be, thus, described in *Ima*2 as constituted by layers of $Co2O_4$ tetrahedra that alternate with layers of $Co1O_6$ octahedra along the *a* axis [Fig. 5(a)]. In the *Ima*2 space group, the orientation of $Co2O_4$ tetrahedra placed at $x=0.25$ and $x=0.75$ is the same (with a shift of (1/2,1/2,1/2) due to the body centering of the unit cell) since they are not related by the inversion symmetry element. The structure contains channels in the tetrahedral planes at $x=0.25$ and $x=0.75$ [Figs. 5(a) and 5(b)] which account for the appreciable oxygen chemical diffusion coefficient[21,22] and high oxygen permeability[23] of this material.

NPD data showed that the magnetic structure is given by the Γ_2 irreducible representation for both 4*a* and 4*b* sites; after the refinement from NPD data the magnetic moments of Co at both positions are arranged in a *G*-type magnetic structure. Unlike the former descriptions of the magnetic structure of $SrCoO_{2.5}$ (Ref. 12) performed in the space group *Icmm*, where the spin direction could not be determined, we clearly and unambiguously refined the spin direction along the *c* axis from NPD data at different temperatures below T_N. In the magnetic structure the magnetic moments are antiferromagnetically coupled within each layer of octahedral units; in the same way every Co atom within the tetrahedral layer is antiferromagnetically coupled with its four nearest Co atoms. Across the *a* direction, the consecutive layers of CoO_6 octahedra placed at $x=0$ and $x=1/2$ are ferromagnetically coupled; the coupling between the layers of tetrahedral units placed at $x=1/4$ and $x=3/4$ is also FM. In principle, the arrangement of the magnetic moments can be understood from the Goodenough-Kanamori rules.[24,25] Within the layer of octahedral units the superexchange path for the Co atoms is Co1-O1-Co1, with bonding angles very close to 180°; for instance, at $T=10$ K this bonding angle is 175.1(6)° (see Table II). Therefore, the expected superexchange interaction between half-occupied, e.g., orbitals is AFM. On the other hand, the superexchange path connecting a Co1 atom of the octahedral layer with the neighboring Co2 atom in the adjacent tetrahedral layer is Co1-O2-Co2, of 156.2(2)° at $T=10$ K, also promoting the AFM interactions. With regard to the coupling of the magnetic moments between the Co2 atoms in the tetrahedral layer, the superexchange path is Co2-O3-Co2 and the bonding angle is far away from 180°; for instance the bonding angle is 116.8(9)° at $T=10$ K [see Table II and Fig. 5(b)]. If the Goodenough-Kanamori rules are considered for the Co2-O3-Co2 superexchange path, the coupling should very probably be FM; however, the AFM coupling found between the nearest Co atoms of the tetrahedral units is indirectly determined from the coupling between the adjacent layers of octahedra and tetrahedra: The interaction between neighboring Co1-Co1 atoms is strongly AFM as well as between Co1-Co2, which determines an AFM coupling between neighboring Co2-Co2 atoms within the tetrahedral layer.

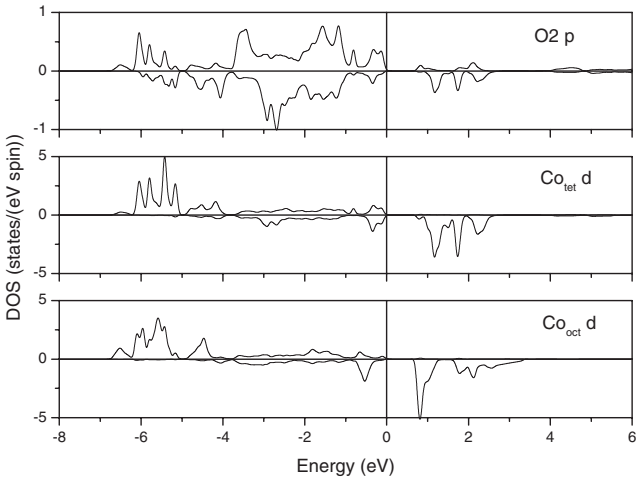

FIG. 10. Density of states for $SrCoO_{2.5}$ in the *Ima*2-based structure. The Co atoms are in a HS $Co^{2+}\underline{L}$ state and the O atoms (O2 *p* levels shown as a representative example) are largely spin-polarized. The upper (lower) panel represents up (down) spin states.

At $T=10$ K. the ordered magnetic moments for Co1 and Co2 atoms are $3.12(13)\mu_B$ and $2.88(14)\mu_B$, respectively, which in both cases is considerably reduced from that expected for Co^{+3} (d^6) in high spin $t_{2g}^4e_g^2$ configuration ($S=2$). The electronic structure calculations also explain the origin of these experimentally observed magnetic moments for the Co atoms. The strong Co (3d)—(2p) hybridization in this charge-transfer insulator leads to the formation of a ligand hole in the surrounding O ions. Hence, the Co atoms are in a $Co^{2+}\underline{L}$ state, where $\underline{L}$ stands for a ligand hole.[26] The magnetic moment of the Co^{2+} cations is only $\sim 3\mu_B$/Co (ideally corresponding to the d^7 configuration) and a very large moment is induced in the O ions, of approximately $0.4\mu_B$/Co. This can be more clearly seen in Fig. 10, showing the density of states (DOS) of both Co atoms and one O atom in the structure. It can be observed that the octahedral Co (lowest panel) ions are in a $t_{2g}^5e_g^2$ state, with the unoccupied t_{2g} state being at 1 eV above the Fermi level, separated by about 1 eV from the higher-lying unoccupied e_g states. A similar $Co^{2+}\underline{L}$ structure can be observed for the tetrahedrally-coordinated Co atom (middle panel), by observing the t_{2g} down-spin band fully unoccupied ($e_g^4t_{2g}^3$ electronic configuration). The large polarization of the O anions can be noticed in the upper panel by observing the depletion of spin-down states close to the Fermi level in the DOS curve of the O2 atom (a similar picture would be found for the other O atoms). The charge-transfer character of the band gap can be noticed by observing the large O *p* character of the states close to the Fermi level and the large Co *d* character of the conduction band.

Another important point concerning the magnetic properties is the broad maximum observed in the ZFC magnetic susceptibility below 200 K (Fig. 2), which is related to the weak ferromagnetism observed in the isothermal magnetization curves (Fig. 4). A similar behavior was previously described for $SrCoO_{2.5}$ by Le Toquin,[27] who proposed that the weak FM component he observed ($0.03\mu_B$) could be induced by a FM interaction in the tetrahedral layers where the superexchange angle is close to 120°. However, the results of the present study of the magnetic structure of $SrCoO_{2.5}$, defined in the *Ima*2 space group, do not allow the existence of a weak ferromagnetism phenomenon for the propagation vector $\mathbf{k}=(1,1,1)$.[28] This can easily be understood as for *Ima*2 the (1/2,1/2,1/2) lattice translation gives rise to an inversion of the magnetic moment direction, in such a way that for each magnetic moment located at a particular (x,y,z) position there is another antiparallel moment at $(x+1/2,y+1/2,z+1/2)$, which cancels any neat magnetization. Instead of a weak ferromagnetism effect, we propose that the anomalies observed in the magnetization curves are originated by the presence of FM clusters of $SrCoO_{3-x}$ embedded in an AFM matrix of $SrCoO_{2.5}$. It is well known, since the former investigations on the $SrCoO_{3-x}$ system, that above 900 °C a cubic phase stabilizes, with the simple-cubic aristotype perovskite structure, which can be identified by high-temperature *in-situ* XRD or NPD techniques.[9,10] This cubic phase has also claimed to be quenched from 1200 °C in liquid N_2 (Ref. 2). On the other hand, this cubic $SrCoO_{3-x}$ perovskite can be alternatively obtained under high pressure conditions.[29] In all cases, the cubic $SrCoO_{3-x}$ phase has been reported to exhibit ferromagnetism below ~200 K, the strength of the FM interactions depending on the oxygen nonstoichiometry and, thus, on the Co^{4+} content, linearly varying from $T_C=180$ K for a sample with 50% Co^{4+} to $T_C=215$ K for a perovskite with 90% Co^{4+}.[30] We propose that in the preparation process of brownmillerite, which is performed by an out-of-equilibrium process by quenching a $SrCoO_{3-x}$ sample in liquid N_2 from 900 °C, clusters of the high-temperature cubic oxygen-deficient phase are trapped and inhomogeneously distributed within the microcrystals.

These clusters are not detected or even detectable by diffraction methods (XRD or NPD), but their imprint is present in the magnetic measurements. On the one hand, these FM regions are sufficiently isolated to be in the origin of the irreversibilities observed between the FC and ZFC curves. On the other hand, the observed reduction of the cusp temperature of the broad peak of the ZFC curves with the applied measuring field, from $T=70$ K at $H=0.1$ kOe to $T=140$ K at 1 kOe resembles the typical response described for superparamagnetic small-particles systems, whose blocking temperature decreases for increasing applied magnetic fields.[31] In our system, this experimental observation constitutes an additional support to the scenario of FM clusters in an AFM matrix, similar to that previously reported in $BaCoO_3$.[32] This is also coherent with the magnetization curves (Fig. 4), at temperatures below and above these susceptibility maxima. We suggest, therefore, that the weak FM signal detected in the magnetization curves is not an intrinsic property of $SrCoO_{2.5}$ brownmillerite, but a result of the presence of FM inhomogeneities. Of course, no anomaly is observed in the thermal evolution of the magnetic structure of $SrCoO_{2.5}$ across the FM T_C of the clusters, since it is an extrinsic phenomenon which does not affect the major AFM matrix.

V. CONCLUSIONS

A study of the crystallographic and magnetic structure of $SrCoO_{2.5}$ from neutron powder diffraction in combination

with *ab-initio* electronic structure calculations allowed us to select the *Ima*2 space group, given the much higher stability of the *Ima*2-based structure with respect to the other possible space group (*Pnma*). The magnetic structure is established below $T_N = 537$ K, with a periodicity given by the propagation vector $k=(1,1,1)$. It is defined by an AFM *G*-type structure with the magnetic moments oriented along the *c* direction. The magnetic structure can be described as AFM layers of CoO_6 octahedra alternating along the *a* direction with AFM layers of CoO_4 tetrahedra; the coupling between the octahedral and tetrahedral layers is AFM. The refined magnetic moments at 10 K, close to $3\mu_B$ at both octahedral and tetrahedral sites, are interpreted as arising from a $Co^{2+}\underline{L}$ state, where $\underline{L}$ stands for a ligand hole. We suggest that the broad maximum and the divergence of FC and ZFC susceptibility curves observed below 200 K arise from the presence of FM clusters of cubic $SrCoO_{3-x}$ perovskite phases (with $T_C \sim 200$ K) embedded into the AFM matrix of $SrCoO_{2.5}$ brownmillerite.

ACKNOWLEDGMENTS

We thank the financial support of CICyT to Projects No. MAT2007–60536 and MAT2006–10027, and we are grateful to ILL for making all facilities available and the CESGA (Centro de Supercomputación de Galicia) for the computing facilities. P.M.B. acknowledges Ministerio de Educación y Ciencia (Spain) for the financial support (J. de la Cierva program).

*Corresponding author; angel.munoz@uc3m.es

[1] J. G. Grenier, S. Ghodbane, G. Demazeau, M. Pouchard, and P. Hagenmuller, Mater. Res. Bull. **14**, 831 (1979).
[2] Y. Takeda, R. Kanno, T. Takada, O. Yamamoto, M. Takano, and Y. Bando, Z. Anorg. Allg. Chem. **540**, 259 (1986).
[3] M. T. Anderson, J. T. Vaughey, and K. R. Poeppelmeier, Chem. Mater. **5**, 151 (1993).
[4] V. V. Vashook, M. V. Zinkevich, and Y. G. Zonov, Solid State Ionics **116**, 129 (1999).
[5] Z. P. Shao and S. M. Haile, Nature (London) **431**, 170 (2004).
[6] P. Bezdicka, J. C. Wattiaux, J. C. Grenier, M. Pouchard, and P. Hagenmuller, Z. Anorg. Allg. Chem. **619**, 7 (1993).
[7] R. Le Toquin, W. Paulus, A. Cousson, C. Prestipino, and C. Lamberti, J. Am. Chem. Soc. **128**, 13161 (2006).
[8] T. Takeda and H. Watanabe, J. Phys. Soc. Jpn. **33**, 973 (1972).
[9] J. Rodríguez, J. M. González-Calbet, J. C. Grenier, J. Pannetier, and M. Anne, Solid State Commun. **62**, 231 (1987).
[10] C. de la Calle, A. Aguadero, J. A. Alonso, M. T. Fernández-Díaz, Solid State Sci. (to be published).
[11] P. Berastegui, S. G. Eriksson, and S. Hull, Mater. Res. Bull. **34**, 303 (1999).
[12] T. Takeda, Y. Yamaguchi, and H. Watanabe, J. Phys. Soc. Jpn. **33**, 970 (1972).
[13] H. M. Rietveld, J. Appl. Crystallogr. **2**, 65 (1969).
[14] J. Rodríguez-Carvajal, J. Phys. B **192**, 55 (1993).
[15] E. Sjöstedt, L. Nördstom, and D. Singh, Solid State Commun. **114**, 15 (2000).
[16] K. Schwarz and P. Blaha, Comput. Mater. Sci. **28**, 259 (2003).
[17] A. I. Liechtenstein, V. I. Anisimov, and J. Zaanen, Phys. Rev. B **52**, R5467 (1995).
[18] J. P. Perdew, K. Burke, and M. Ernzerhof, Phys. Rev. Lett. **77**, 3865 (1996).
[19] D. Singh, *Planewaves, Pseudopotentials and the LAPW Method* (Kluwer, Dordrecht, 1994).
[20] E. F. Bertaut, Acta Crystallogr., Sect. A: Cryst. Phys., Diffr., Theor. Gen. Crystallogr. **24**, 217 (1968).
[21] M. V. Zinkevich and V. V. Vashook, Elektrokhimiya **28**, 1800 (1992).
[22] M. V. Zinkevich and V. V. Vashook, Vestsi Akad. Navuk Belarusi, Ser. Fiz.-Mat. Navuk **3**, 48 (1993).
[23] H. Kruidhof, H. J. M. Bovwmeester, F. H. E. Doorn, and A. J. Burggraaf, Solid State Ionics **63–65**, 816 (1993).
[24] J. B. Goodenough, Phys. Rev. **100**, 564 (1955).
[25] J. Kanamori, J. Phys. Chem. Solids **10**, 87 (1959).
[26] M. A. Korotin, S. Yu. Ezhov, I. V. Solovyev, V. I. Anisimov, D. I. Khomskii, and G. A. Sawatzky, Phys. Rev. B **54**, 5309 (1996).
[27] R. Le Toquin, Ph.D. thesis, University of Rennes (France), 2003.
[28] E. A. Turov, *Physical Properties of Magnetically Ordered Crystals* (Academic, New York, 1965).
[29] H. Taguchi, M. Shimada, and M. Koizumu, J. Solid State Chem. **40**, 42 (1981).
[30] H. Taguchi, M. Shimada, and M. Koizumu, J. Solid State Chem. **29**, 221 (1979).
[31] P. M. Botta, V. Pardo, D. Baldomir, C. de la Calle, J. A. Alonso, and J. Rivas, Phys. Rev. B **74**, 214415 (2006).
[32] J. L. Dormann, D. Fiorani, and E. Tronc, Adv. Chem. Phys. **98**, 283 (1997).